JOURNAL OF GEOPHYSICAL RESEARCH: SPACE PHYSICS, VOL. 118, 794–803, doi:10.1002/jgra.50124, 2013

Two models of cross polar cap potential saturation compared: Siscoe-Hill model versus Kivelson-Ridley model

Ye Gao,[1,2] Margaret G. Kivelson,[1,2,3] and Raymond J. Walker[1,2]

Received 16 October 2012; revised 4 January 2013; accepted 10 January 2013; published 28 February 2013.

[1] The cross polar cap potential is considered an instantaneous monitor of the rate at which magnetic flux couples the solar wind to the Earth's magnetosphere-ionosphere system. Studies have shown that the cross polar cap potential responds linearly to the solar wind electric field under nominal solar wind conditions but asymptotes to the order of 200 kV for large electric field. Saturation of the cross polar cap potential is also found to occur in MHD simulations. Several mechanisms have been proposed to explain this phenomenon. Two well-developed models are those of *Siscoe et al*. (2002), herein referred to as the Siscoe-Hill model, and of *Kivelson and Ridley* (2008), herein referred to as the Kivelson-Ridley model. In this study, we compare the mathematical formulas as well as the predictions of the two models with data. We find that the two models predict similar saturation limits. Their difference can be expressed in terms of a factor, which is close to unity during a saturation interval. A survey of the differences in the model predictions show that, on average, the potential of the Kivelson-Ridley model is smaller than that of the Siscoe-Hill model by 10 kV. Measurements of AMIE, DMSP, PC index, and SuperDARN are used to differentiate between the two models. However, given the uncertainties of the measurements, it is impossible to conclude that one model does a better job than the other of predicting the observed cross polar cap potentials.

Citation: Gao, Y., M. G. Kivelson, and R. J. Walker (2013), Two models of cross polar cap potential saturation compared: Siscoe-Hill model versus Kivelson-Ridley model, *J. Geophys. Res. Space Physics*, *118*, 794–803, doi:10.1002/jgra.50124.

1. Introduction

[2] The cross polar cap potential (Φ_{PC}) measures the rate of magnetic flux transfer from the solar wind to the Earth's magnetosphere-ionosphere system. It is an important parameter in characterizing the coupling among solar wind, magnetosphere, and ionosphere. *Boyle et al.* [1997] empirically obtained a formula that linearly relates Φ_{PC} measured by Defense Meteorological Satellite Program (DMSP) to the solar wind parameters through

$$\Phi_{PC}[\mathrm{kV}] \approx 10^{-7}u[\mathrm{km/s}]^2 + 11.7B[\mathrm{nT}]\sin^3(\theta/2), \quad (1)$$

where Φ_{PC} is in kV, u is the solar wind velocity in km/s, and B is the magnitude of the interplanetary magnetic field (IMF) in nT. *Boyle et al.* [1997] attributed the first term to the viscous interaction between the solar wind and the magnetosphere through the low-latitude boundary layer, i.e.,

$$\Phi_{vis}[\mathrm{kV}] \approx 10^{-7}u[\mathrm{km/s}]^2, \quad (2)$$

and the second term to low-latitude magnetic reconnection, i.e.,

$$\Phi_{rec}[\mathrm{kV}] \approx 11.7B[\mathrm{nT}]\sin^3(\theta/2). \quad (3)$$

Previous studies found that Φ_{PC} predicted from equation (1) agrees reasonably well with observations under nominal solar wind conditions [*Boyle et al*., 1997; *Jiang et al*., 2011; *Gao*, 2012a]. However, under intense solar wind driving, Φ_{PC} reaches an upper limit or saturates [e.g., *Russell et al*., 2000], instead of increasing linearly as predicted by equation (1). The saturation of Φ_{PC} is consistent with observations [e.g., *Nagatsuma*, 2002; *Shepherd et al*., 2002; *Hairston et al*., 2003; *Ober et al*., 2003] and is found to occur in MHD simulations [e.g., *Raeder et al*., 2001; *Siscoe et al*., 2002; *Merkine et al*., 2003]. Several models have been proposed to explain the saturation of Φ_{PC} [*Siscoe et al*., 2002; *Siscoe et al*., 2004; *Kivelson and Ridley*, 2008; *Borovsky et al*., 2009]. However, the physical mechanism is still in debate. *Borovsky et al.* [2009] compared several saturation models and categorized them as reconnection and postreconnection models. The reconnection models, with details varying, explain the reduced potential as being caused by a reduction of the dayside reconnection rate [*Raeder et al*., 2001; *Siscoe et al*., 2002; 2004; *Merkin et al*., 2005; *Ridley*, 2005]. In contrast, the postreconnection model of *Kivelson and Ridley* [2008] explains the reduced potential in terms of processes occurring on the newly reconnected field lines.

[1]Department of Earth and Space Sciences, UCLA, Los Angeles, California, USA.
[2]Institute of Geophysics and Planetary Physics, UCLA, Los Angeles, California, USA.
[3]Department of Atmospheric, Oceanic and Space Sciences, University of Michigan, Ann Arbor, Michigan, USA.

Corresponding author: Y. Gao, Department of Earth and Space Sciences, UCLA, Los Angeles, CA, USA. (ygao@igpp.ucla.edu)

2169-9380/13/10.1002/jgra.50124

[3] The most extensively studied reconnection model is presented by *Siscoe et al.* [2002; 2004], herein referred as the Siscoe-Hill model [*Hill et al.*, 1976; *Siscoe et al.*, 2002; 2004]. The Siscoe-Hill model explains the saturation of Φ_{PC} as a result of the feedback of the Region 1 current. Under extreme solar wind driving, the magnetic field generated by the Region 1 current becomes comparable to and opposes the Earth's dipole field at the magnetopause where reconnection occurs. By significantly weakening the field that is reconnecting, the Region 1 current ultimately limits the reconnection rate, resulting in the saturation of Φ_{PC} [*Siscoe et al.*, 2002].

[4] *Hill et al.* [1976] argued that, for any given solar wind reconnection electric field, the cross polar cap potential is determined by the interplay between an unsaturated transmagnetospheric potential (Φ_M) and a saturated transpolar potential (Φ_S). Φ_M is the potential drop around the magnetopause that results from magnetic reconnection in the absence of the saturation mechanism. This is an idealized potential in that the model assumes that it increases linearly with the reconnection electric field ($E_{K\text{-}L}$) [*Kan and Lee*, 1979], i.e.,

$$\Phi_M \propto E_{K-L}, \tag{4}$$

even in the saturation domain where, according to the model, the real reconnection potential drop saturates. Here $E_{K\text{-}L}$ is related to the solar wind parameters through

$$E_{K-L} = uB_{YZ}\sin^2(\theta/2), \tag{5}$$

where u is the solar wind velocity,

$$B_{YZ} = \left(B_Y{}^2 + B_Z{}^2\right)^{1/2} \tag{6}$$

in the GSM coordinates, and θ is the interplanetary magnetic field (IMF) clock angle measured clockwise from the GSM Z axis in a plane perpendicular to the Earth-Sun line. Φ_S is the transpolar potential that generates Region 1 current strong enough to prevent any further increase in the reconnection rate by creating an opposing magnetic field at the reconnection site. *Hill et al.* [1976] expressed the interplay between Φ_M and Φ_S by combining them as

$$\Phi_{S-H} = \Phi_M\Phi_S/(\Phi_M + \Phi_S). \tag{7}$$

Under nominal solar wind conditions, $\Phi_M \ll \Phi_S$. Thus,

$$\Phi_{S-H} \approx \Phi_M. \tag{8}$$

However, at high levels of geomagnetic activity, Φ_M increases to such an extent that $\Phi_M \gg \Phi_S$ and

$$\Phi_{S-H} \approx \Phi_S. \tag{9}$$

Thus, $\Phi_{S\text{-}H}$ saturates for these intervals. *Siscoe et al.* [2002] adopted and extended the results of *Hill et al.* [1976] by relating Φ_M and Φ_S to solar wind and ionospheric parameters. *Siscoe et al.* [2002] applied magnetic reconnection theory to the magnetopause and obtained an analytical formula for Φ_M as

$$\Phi_M = 1.82 \times 10^6 E_{K-L}p^{-1/6}, \tag{10}$$

where $E_{K\text{-}L}$ is the reconnection electric field [*Kan and Lee*, 1979] and p is the solar wind pressure in SI units. In the following analysis, the parameters are in SI units. p, in equation (10), includes both the solar wind dynamic pressure (p_{dyn}) and the magnetic pressure (p_{mag}), i.e.,

$$p = p_{dyn} + p_{mag}. \tag{11}$$

Here

$$p_{dyn} = \rho u^2, \text{and} \quad p_{mag} = B^2/2\mu_0, \tag{12}$$

where ρ is the solar wind mass density, B is the IMF magnitude, and $\mu_0 = 4\pi \times 10^{-7}$ H/m is the permeability of free space.

[5] The analytic formula for Φ_S is derived based on the magnetic field generated by the Region 1 current and is given by

$$\Phi_S = 4.61 \times 10^9 p^{1/3}/\xi\Sigma_P, \tag{13}$$

where Σ_P, fixed at 10 S, is the ionospheric Pedersen conductance and ξ is a coefficient of the geometry of current flow lines in the ionosphere. An empirical equation given by *Siscoe et al.* [2002] relates ξ to Σ_P through

$$\xi \approx 4.45 - 1.08\log_{10}\Sigma_P. \tag{14}$$

From equation (14), ξ, usually between 3 and 4, is not sensitive to Σ_P. When Σ_P = 10 S, ξ = 3.37, which is the value used in the following analysis. To emphasize,

$$\xi|_{\Sigma_P=10\ S} = 3.37. \tag{15}$$

By substituting equation (10) and equation (13) into equation (7), the analytic formula of the Siscoe-Hill model is obtained, i.e.,

$$\Phi_{S-H} = \Phi_{vis} + 1.82 \times 10^6 E_{K-L}p^{1/3}/\left(p^{1/2} + 4 \times 10^{-4}\xi\Sigma_P E_{K-L}\right). \tag{16}$$

where a viscous term has been added.

[6] The model of *Kivelson and Ridley* [2008], i.e., Kivelson-Ridley model, is considered as a postreconnection model because it places no constraints on the reconnection efficiency or the magnetospheric geometry. *Kivelson and Ridley* [2008] argued that. when the impedance of the solar wind across polar cap field lines dominates the impedance of the ionosphere, the Alfvén waves incident from the solar wind are partially reflected, reducing the signal in the polar cap. The ratio of the cross polar cap electric field ($E_{K\text{-}R}$) to the reconnection electric field ($E_{K\text{-}L}$) is $2\Sigma_A/(\Sigma_P+\Sigma_A)$, i.e.,

$$E_{K-R} = E_{K-L}2\Sigma_A/(\Sigma_P + \Sigma_A), \tag{17}$$

where Σ_P is the ionospheric Pederson conductance taken as 10 S, and Σ_A, the Alfvén conductance of the solar wind, is computed from

$$\Sigma_A = 1/\mu_0 v_A, \tag{18}$$

and

$$v_A = B/(\mu_0\rho)^{1/2}. \tag{19}$$

Under nominal solar wind conditions, $\Sigma_A \approx 16$ S. With $\Sigma_P \approx 10$ S [*Kivelson and Ridley*, 2008], $E_{K\text{-}R}$ is slightly larger than but close to $E_{K\text{-}L}$, i.e.,

$$E_{K-R} \approx 1.2 E_{K-L}. \tag{20}$$

Under intense solar wind driving, Σ_A decreases to such an extent that $\Sigma_A < \Sigma_P$. Therefore,

$$E_{K-R} < E_{K-L}. \tag{21}$$

Then, the cross polar cap potential is calculated from

$$\Phi_{K-R} = \Phi_{vis} + E_{K-R} D, \tag{22}$$

where D is defined as the distance across the unperturbed solar wind containing field lines that reconnect as they encounter the dayside of the magnetosphere. D is taken to be proportional to the distance to the nose of the magnetopause (R_{mp}),

$$D = 0.1 R_{mp}, \tag{23}$$

where R_{mp} is calculated from

$$R_{mp} = \left[(2B_0)^2/2\mu_0 p\right]^{1/6} R_E, \tag{24}$$

where B_0 = 30.4 μT is the equatorial surface field of the Earth. Thus, the analytic formula given by the Kivelson-Ridley model is

$$\Phi_{K-R} = \Phi_{vis} + 1.35 \times 10^6 E_{K-L} p^{-1/6} \Sigma_A/(\Sigma_A + \Sigma_P), \tag{25}$$

where

$$0.2\pi\left[(2B_0)^2/2\mu_0\right]^{1/6} R_E = 1.35 \times 10^6 \tag{26}$$

has been substituted. In this paper, we explore the similarities and differences between these two models and compare the model predictions with measurements. In section 2, we compare equation (16) with equation (25) in the saturation limit. We find that, except for some trivial differences, equation (16) is practically the same as equation (25) in the saturation limit. In section 3, using the same cases as *Gao et al.* [2012c], the model predictions are compared to the measurements of AMIE, DMSP, PC index, and SuperDARN. Since different measurements give very different values, but the model predictions are close, it is impossible to show that one model is better than the other by comparing the predictions with the measurements.

2. A Formula of $\Phi_{S\text{-}H}$ Similar to $\Phi_{K\text{-}R}$

[7] In this section, we compare equation (16) with equation (25) under nominal solar wind conditions. First, we notice that by defining

$$F = 2.5 \times 10^3 p^{1/2}/\xi E_{K-L}, \tag{27}$$

equation (16) can be written in a form similar to equation (25), i.e.,

$$\Phi_{S-H} = \Phi_{vis} + 1.82 \times 10^6 E_{K-L} p^{-1/6} F/(F + \Sigma_P), \tag{28}$$

with the major difference that F in equation (28) replaces Σ_A in equation (25). To relate F to Σ_A, we define

$$0.74\eta = F/\Sigma_A, \tag{29}$$

where 0.74 is 1.35×10^6 divided by 1.82×10^6. By substituting equation (18)and equation (27) into equation (29), we obtain

$$\eta = 2.5 \times 10^3 p^{1/2} \mu_0 v_A / 0.74 \xi E_{K-L}. \tag{30}$$

Then, we substitute equation (5) and equation (19) into equation (30), and arrive at

$$\eta = \left(2.5 \times 10^3 {\mu_0}^{1/2}/0.74\xi\right)\left(p^{1/2}/\rho^{1/2}u\right)(B/B_{YZ}) \sin^{-2}(\theta/2). \tag{31}$$

Furthermore, by using $2.5 \times 10^3 \mu_0^{1/2}/0.74\xi \approx 1$, equation (31) can be reduced to

$$\eta \approx \left(1 + p_{mag}/p_{dyn}\right)^{1/2}(B/B_{YZ}) \sin^{-2}(\theta/2) \tag{32}$$

Thus, η varies between 1 and ∞, i.e.,

$$\eta \in (1, \infty). \tag{33}$$

In equation (32), ξ is estimated by substituting Σ_P = 10 S in equation (14), i.e., ξ = 3.37. In summary,

$$\Phi_{S-H} = \Phi_{vis} + 1.34 \times 10^6 E_{K-L} p^{-1/6} \eta \Sigma_A/(0.74\eta\Sigma_A + \Sigma_P). \tag{34}$$

Thus, the challenge is to distinguish the above equation from

$$\Phi_{K-R} = \Phi_{vis} + 1.35 \times 10^6 E_{K-L} p^{-1/6} \Sigma_A/(\Sigma_A + \Sigma_P). \tag{35}$$

The saturation of cross polar cap potential often occurs concurrently with a magnetic storm driven by a coronal mass ejection (CME) [e.g., *Kivelson and Ridley*, 2008], during which Σ_A can decrease to such an extent that

$$\Sigma_A \ll \Sigma_P, \tag{36}$$

In this limit,

$$\Sigma_A + \Sigma_P \approx \Sigma_P, \text{and } 0.74\Sigma_A + \Sigma_P \approx \Sigma_P. \tag{37}$$

Under nominal solar wind conditions, B_X is usually comparable to or larger than B_Z in magnitude due to the Parker spiral. In fact, 1 min ACE data show that $|B_X| > |B_Z|$ is satisfied 61.8% of the time from 1999 to 2009. However, during exceptionally disturbed periods, the field configuration is typically abnormal. Frequently, saturation is associated with the passage of a CME. For such an interval, B_Z usually dominates over both B_X and B_Y, i.e.,

$$|B_Z| \gg |B_Y|, \text{and } |B_Z| \gg |B_X|. \tag{38}$$

For these conditions,

$$B/B_{YZ} \approx 1, \text{and } \sin^{-2}(\theta/2) \approx 1. \tag{39}$$

Furthermore, if we assume

$$1 + p_{mag}/p_{dyn} \approx 1, \text{or } p \approx p_{dyn}, \tag{40}$$

then

$$\eta \approx 1. \quad (41)$$

Ignoring the viscous term, $\Phi_{S\text{-}H}$ and $\Phi_{K\text{-}R}$ become

$$\Phi_{S-H} \approx 1.20 \times 10^9 p^{1/3}/\Sigma_P, \text{and } \Phi_{K-R} \approx 1.20 \times 10^9 p^{1/3}/\Sigma_P, \quad (42)$$

and it follows that

$$\Phi_{S-H} \approx \Phi_{K-R}. \quad (43)$$

In equation (42),

$$E_{K-L}\Sigma_A = \left(uB_{YZ}\sin^2\theta/2\right)\left(\rho^{1/2}/B{\mu_0}^{1/2}\right) \approx 892p^{1/2} \quad (44)$$

has been used in both forms of the cross polar cap potential.

[8] The preceding analysis demonstrates that the Siscoe-Hill model and the Kivelson-Ridley model predict similar saturated potentials for solar wind conditions that lead to saturation. In order to obtain significantly different predictions from the two models, η needs to be larger than 1, requiring a large B_X (so that B/B_{YZ} differs significantly from 1), or $p_{\rm mag}$ must be comparable to $p_{\rm dyn}$. Neither of these situations is typical of the solar wind conditions that drive the polar cap into saturation.

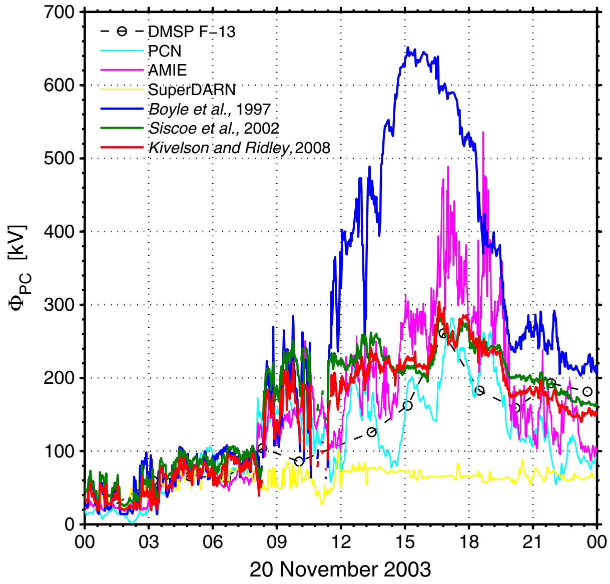

Figure 1. The cross polar cap potential (Φ_{PC}) on 20 November 2003. The blue line is Φ_{PC} computed from equation (1). The green line is $\Phi_{S\text{-}H}$. The red line is $\Phi_{K\text{-}R}$. The black dashed line with circles is Φ_{PC} measured by DMSP. The cyan line is Φ_{PC} converted from PC index by using the formula of *Troshichev et al.* [1996]. The magenta line is Φ_{PC} measured by AMIE. The yellow line is Φ_{PC} measured by SuperDARN.

3. Comparing Model Predictions With Measurements

[9] Four techniques are commonly used to infer the ionospheric parameters from which the cross polar cap potential is determined [*Gao*, 2012a]. Assimilative Mapping of Ionospheric Electrodynamics (AMIE) uses magnetic field data from ground magnetometers and electric field data from radars and satellites to map high-latitude electrostatic potentials, from which the difference of the potential extrema is used to estimate Φ_{PC} [*Richmond and Kamide*, 1988; *Richmond et al.*, 1988]; Defense Meteorological Satellite Program (DMSP) measures the cross-track ion drift velocity and estimates Φ_{PC} from the difference of the potential extrema along the spacecraft trajectory [*Hairston et al.*, 1998]; the polar cap (PC) index is derived from the surface magnetic field perturbation [*Troshichev et al.*, 1988] and is found to relate to Φ_{PC} through the formula of *Troshichev et al.* [1996], i.e.,

$$\Phi_{PC}[\text{kV}] \approx 19.35\text{PC} + 8.78; \quad (45)$$

(see also *Ridley and Kihn* [2004] for a different formula to convert from the PC index to Φ_{PC}). The Super Dual Auroral Radar Network (SuperDARN) measures the line-of-sight ionospheric convection velocities with a ground-based network of radars and then infers the electrostatic potential pattern from the convection velocity observations. Φ_{PC} is obtained from the difference between the potential extrema [*Ruohoniemi and Baker*, 1998].

[10] Using the saturation events of *Gao et al.* [2012c], we compare the potentials predicted from equations (16) and (25) with the measurements. The solar wind inputs for the two equations are taken from the measurements of the Advanced Composite Explorer (ACE) spacecraft. The technique of *Weimer et al.* [2003] and *Weimer* [2004] is used to propagate the data from Lagrange point 1 ($L1$) to $X_{\rm GSM} = 17R_{\rm E}$. Figure 1 shows an example from 20 November 2003. Φ_{PC} predicted from equation (1), equation (16), and equation (25) are displayed with the blue line, the green line, and the red line, respectively. Φ_{PC}s measured by the aforementioned techniques are also plotted. For consistency, we define saturation as the time interval during which the formula of *Boyle et al.* [1997] (equation (1)) overpredicted Φ_{PC} by at least 100 kV compared to the second largest prediction or measurement. This occurred between 11:00 UT and 20:00 UT for this case. From Figure 1, it is clear that, during the saturation interval, different techniques can give quite different measurements. For example, Φ_{PC} measured by SuperDARN is significantly lower than the values obtained from other techniques. However, the model predictions of $\Phi_{S\text{-}H}$ and $\Phi_{K\text{-}R}$ agree well with each other.

[11] As argued by *Siscoe et al.* [2002], the transmagnetospheric potential Φ_M dominated the transpolar potential Φ_S during the saturation interval (Figure 2a). Thus, in this interval, $\Phi_{S\text{-}H}$ was almost equal to Φ_S. At the same time, as seen from Figure 2b, Σ_A decreased to such an extent that $\Sigma_A < \Sigma_P$ was satisfied as suggested by *Kivelson and Ridley* [2008]. Therefore, $E_{K\text{-}R}$ became smaller than $E_{K\text{-}L}$. Figure 3 compares the relative magnitudes of B_X and B_Z for this event. As shown in Figure 3a, $|B_Z/B_X|$ was consistently above 1 and close to 5 after 12:00 UT, which indicates that $|B_Z| \gg |B_X|$. The dominance of $|B_Z|$ over $|B_X|$ is confirmed by examining the time series of $|B_Z| - |B_X|$, which is shown in Figure 3b. Clearly, $|B_Z| - |B_X|$ stayed positive after 12:00 UT.

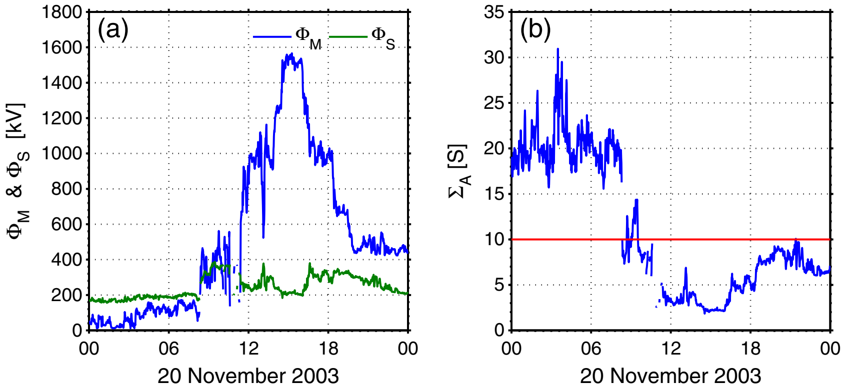

Figure 2. The parameters of Siscoe-Hill model and Kivelson-Ridley model on 20 November 2003. (a) The transmagnetospheric potential Φ_M (equation (10)) and the transpolar potential Φ_S (equation (13)). (b) The Alfvén conductance of the solar wind, Σ_A (equation (18)). The red line in Figure 2b labels 10 S, which is the value of Σ_P used in this study.

Similarly, $|B_Z|$ also dominated over $|B_Y|$ after 12:00 UT, i.e., $|B_Z| \gg |B_Y|$ (not shown here). Besides, we calculate the ratio of $|B_Z|$ over $|B_X|$ for saturation intervals satisfying Φ_{PC} derived from the PC index (equation (45)) larger than 150 kV for all the cases, and find that, on average, $|B_Z| \approx 3.5|B_X|$ for such intervals. Figure 4 compares the magnetic pressure p_{mag} with the dynamic pressure p_{dyn} for this case. As seen from Figure 4a, on 20 November 2003, p_{dyn} was always larger than p_{mag}. The ratio, p_{dyn}/p_{mag}, was close to 100 during the nonsaturation interval (00:00 UT to 09:00 UT in Figure 4b). Even though the ratio decreased during the saturation interval, it remained above 3. Thus, it is legitimate to assume that equation (40) is satisfied and that similar predictions from equations (34) and (35) can be expected.

[12] Another case on 6–7 April 2000 is shown in Figure 5. The formula of *Boyle et al.* [1997] overpredicted Φ_{PC} in the interval between 18:00 UT and 24:00 UT on 6 April 2000. As in the previous case, $\Phi_{S\text{-}H}$ was close to $\Phi_{K\text{-}R}$, while substantial differences between the observations were found during the saturation interval. A detailed examination of the other events of *Gao et al.* [2012c] supports our finding that $\Phi_{S\text{-}H}$ and $\Phi_{K\text{-}R}$ are close while there are larger differences in the observations. Because of lack of midlatitude radars before 2005, the SuperDARN radars' limited field of view was not able to cover the whole polar cap in a saturation interval, and thus, its measurements appeared systematically to underestimate Φ_{PC}. It has been shown that recent deployment of SuperDARN radars at midlatitude expanded the SuperDARN equatorward and provided data for more precise estimation of convection distribution at high levels of geomagnetic activity, both on statistical basis [*Baker et al.*, 2007] and on an event basis [*Ebihara et al.*, 2009]. The SuperDARN measurements are included in this study for completeness. However, we rely on the measurements of AMIE, DMSP, and the PC index to differentiate the two models. The difference between Φ_{PC} inferred from AMIE ($\Phi_{PC,AMIE}$) and that inferred from the PC index ($\Phi_{PC,PC}$), i.e., $\Phi_{PC,AMIE} - \Phi_{PC,PC}$, in 2000 is shown in Figure 6a. In general, the difference between the two techniques is close to 10 kV. However, for a saturation interval, it is common for the difference to increase to 100 kV (e.g., Figure 6b). The differences between Φ_{PC} inferred from AMIE and that inferred from DMSP, and between Φ_{PC} inferred from DMSP and that inferred from the PC index are also on the order of 100 kV for a saturation interval (e.g., Figure 1).

[13] Using 1 min observations from the Advanced Composition Explorer (ACE) to evaluate equation (35), a histogram of $\Phi_{K\text{-}R}$ from 1999 to 2009 is shown in Figure 7a. The probability mass concentrates around 30 kV and predicted values larger than 150 kV rarely occur. *Kivelson and Ridley* [2008] argue that saturation occurs when the impedance of the solar wind dominates that of the ionosphere, i.e.,

$$\Sigma_A < \Sigma_P. \tag{46}$$

With Σ_P fixed at 10 S, this saturation criterion, i.e., $\Sigma_A < 10$ S, is met 6% of the time (Figure 7b). In Figure 7c, the histogram of $\Phi_{S\text{-}H}$ is displayed. Compared to Figure 7a, $\Phi_{S\text{-}H}$ is likely to

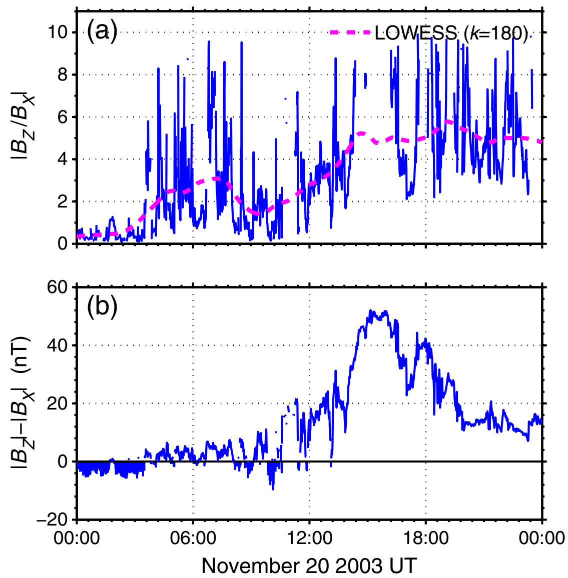

Figure 3. The relative magnitude of IMF B_X and B_Z on 20 November 2003. (a) $|B_Z / B_X|$ versus time. (b) $|B_Z| - |B_X|$ versus time. The magenta dashed line in Figure 3a is computed by smoothing the blue solid line using the technique of LOWESS with window length 180 [*Cleveland*, 1979].

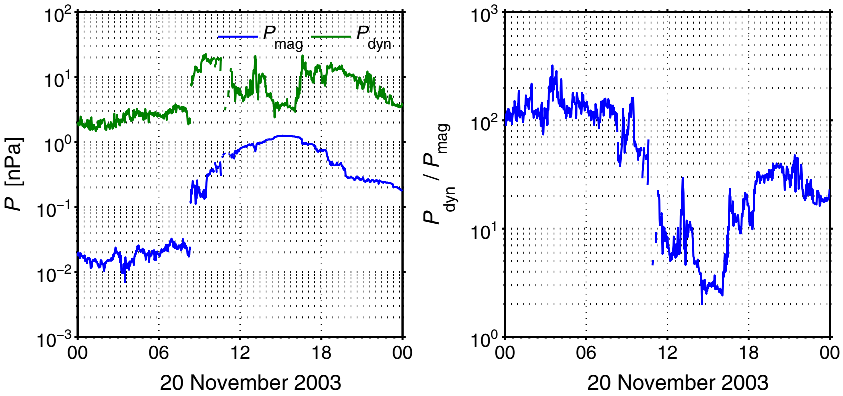

Figure 4. The magnetic pressure p_{mag} and dynamic pressure p_{dyn} on 20 November 2003. (a) p_{mag} and p_{dyn} versus time. (b) The ratio between p_{dyn} and p_{mag} versus time. The Y axes are in logarithmic scales.

take on a value larger than $\Phi_{K\text{-}R}$. *Siscoe et al.* [2002] argued that when the transmagnetospheric potential (Φ_M) dominates the transpolar potential (Φ_S), saturation occurs, which results in the saturation criterion,

$$\Phi_M > \Phi_S. \tag{47}$$

For the solar wind observations from 1999 to 2009, this criterion is satisfied 4% of the time (Figure 7d).

[14] The difference between $\Phi_{K\text{-}R}$ and $\Phi_{S\text{-}H}$ is systematically examined by studying

$$\Delta = \Phi_{K-R} - \Phi_{S-H}, \tag{48}$$

from 1999 to 2009. A histogram of Δ is shown in Figure 8a. Notice that the distribution of Δ is strongly biased toward the negative end, which means that, in general,

$$\Phi_{K-R} \leq \Phi_{S-H}. \tag{49}$$

The probability mass of Δ concentrates around 10 kV, i.e.,

$$\Phi_{S-H} \approx \Phi_{K-R} + 10\ \text{kV}. \tag{50}$$

Given the uncertainties of measurements, a difference of 10 kV is not large enough to differentiate the two models. The conditional distribution of Δ under

$$\Phi_M > \Phi_S \tag{51}$$

is shown in Figure 8b. Compared to Figure 8a, the difference between $\Phi_{K\text{-}R}$ and $\Phi_{S\text{-}H}$ is more likely to take on a large (negative) value for cases in which $\Phi_{S\text{-}H}$ satisfies saturation conditions. The criterion,

$$\Sigma_A < 10\ \text{S}, \tag{52}$$

(for which $\Phi_{K\text{-}R}$ predicts saturation) can also be used to demonstrate the same inequality as is shown in Figure 8c. Figure 8d shows the distribution of Δ when both criteria are used. Regardless of the particular form used as a saturation criterion (Figures 8b, 8c, or 8d), the magnitude of the difference between the two predictions increases when data are restricted to saturated intervals (e.g., $\Phi_M > \Phi_S$, or $\Sigma_A < 10$ S). However, there are still very few cases for which $\Phi_{K\text{-}R}$ differs from $\Phi_{S\text{-}H}$ substantially. For example, in the decade analyzed, there is only one case, on 15 May 2005, with intervals during which,

$$|\Delta| > 100\ \text{kV}. \tag{53}$$

We next examine the data for this special case.

[15] The case of 15 May 2005 is shown in Figure 9. After 06:00 UT, the difference between $\Phi_{S\text{-}H}$ and $\Phi_{K\text{-}R}$ remained close to 100 kV for the remainder of the day. The reason for the difference between $\Phi_{K\text{-}R}$ and $\Phi_{S\text{-}H}$ is revealed in Figure 10. After 06:00 UT, Σ_A was much smaller than Σ_P, i.e., $\Sigma_A \ll \Sigma_P$ (Figure 10f). Corresponding to the big difference between $\Phi_{K\text{-}R}$ and $\Phi_{S\text{-}H}$ during the interval with $\Sigma_A < \Sigma_P$ (Figure 10a), η differs substantially from 1 (Figure 10b) due to the IMF geometry (Figure 10c), for which $B/B_{YZ}\sin^{-2}\theta/2$ became large (Figure 10d). Although p_{mag} was close to p_{dyn} at around 10:00 UT, the ratio of p_{mag} to p_{dyn} remained below 1 (Figure 10e) and thus did not contribute to η significantly. Thus, again ignoring the viscous term,

$$\Phi_{K-R} \approx 1.35 \times 10^6 E_{K-L} p^{-1/6} \Sigma_A/\Sigma_P, \tag{54}$$

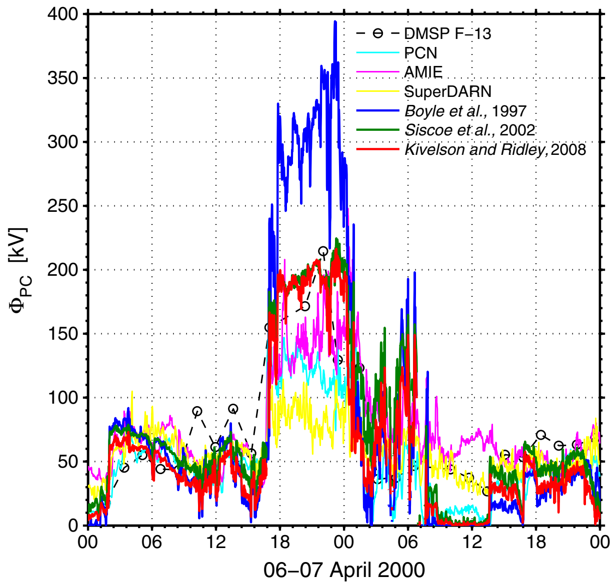

Figure 5. As in Figure 1 for a different case on 6–7 April 2000.

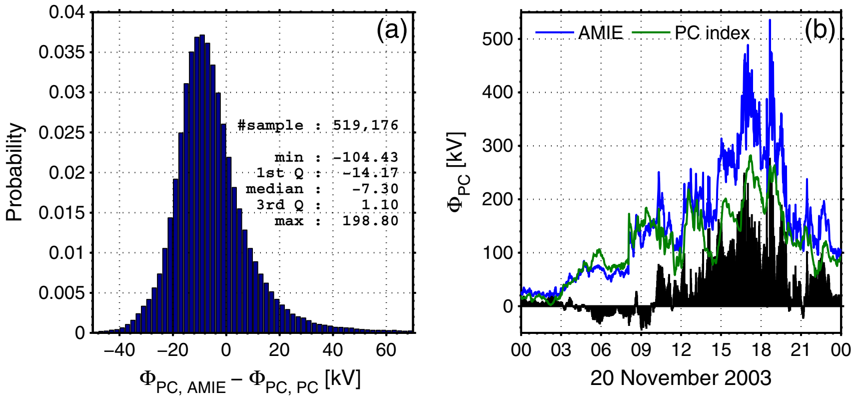

Figure 6. (a) Histogram of the difference between Φ_{PC} inferred from AMIE ($\Phi_{PC,AMIE}$) and Φ_{PC} inferred from the PC index ($\Phi_{PC,PC}$) in 2000. The distribution is summarized as follows: minimum, –104.43; first quartile, –14.17; median, –7.30; third quartile, 1.10; maximum, 198.80. (b) Time series of Φ_{PC} inferred from AMIE (blue line), Φ_{PC} inferred from the PC index (green line), and their difference (black area) in 20 November 2003.

and,

$$\Phi_{S-H} \approx 1.82 \times 10^6 E_{K-L} p^{-1/6} = \Phi_M. \quad (55)$$

In other words, for the interval between 09:00 UT and 18:00 UT when IMF was northward-oriented, the theory of *Kivelson and Ridley* [2008] predicts saturation of cross polar cap potential, while, according to *Siscoe et al.* [2002, 2004], saturation did not occur. Clearly, after 09:00 UT, the measurements were close to Φ_{K-R} in terms of absolute value. However, the measured Φ_{PC} was much smaller than both Φ_{S-H} and Φ_{K-R} from 06:00 UT to 08:00 UT. One should note that, after 06:00 UT, the time derivative of Φ_{PC} measured by AMIE or PC index was closer to the derivative of Φ_{S-H} than the derivative of Φ_{K-R} (i.e., $\Phi_{S-H} - \Phi_{PC} \approx$ const). In summary, the measurements favor Φ_{K-R} in terms of absolute value but favor Φ_{S-H} in terms of time derivative. Thus,

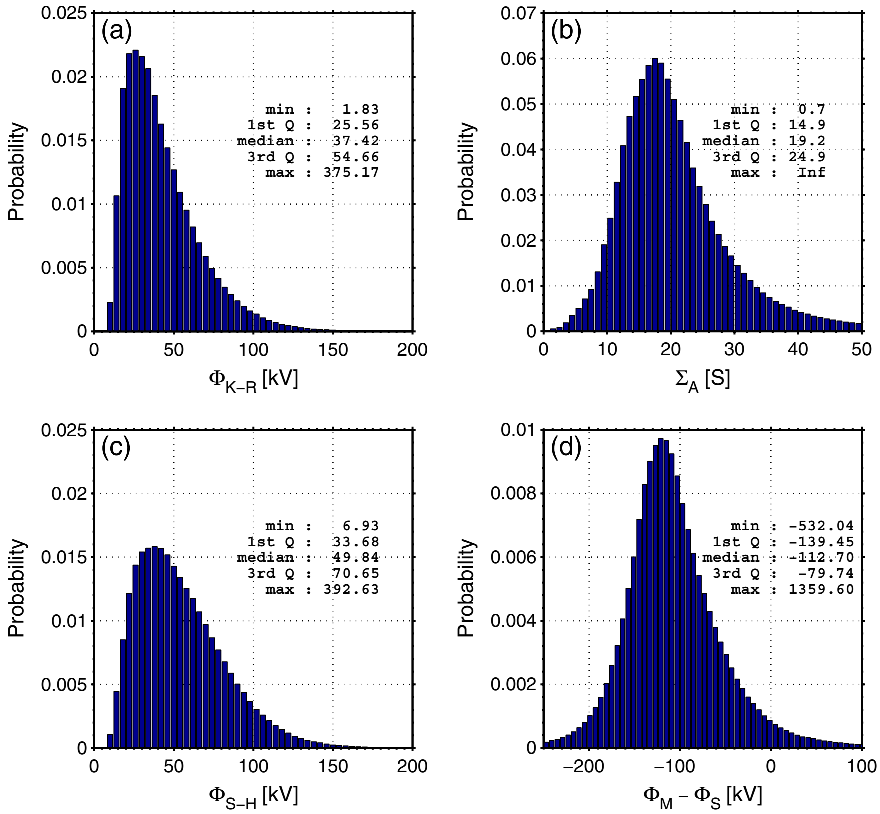

Figure 7. Histograms of Φ_{K-R} (a), Σ_A (b), Φ_{S-H} (c), and $\Phi_M - \Phi_S$ (d) for 1 min solar wind observation from 1999 to 2009. The text in a panel shows the summary statistics of the plotted quantity. For example, in Figure 7a, Φ_{K-R} is summarized as follows: minimum, 1.83; first quartile, 25.56; median, 37.42; third quartile, 54.66; maximum, 375.17.

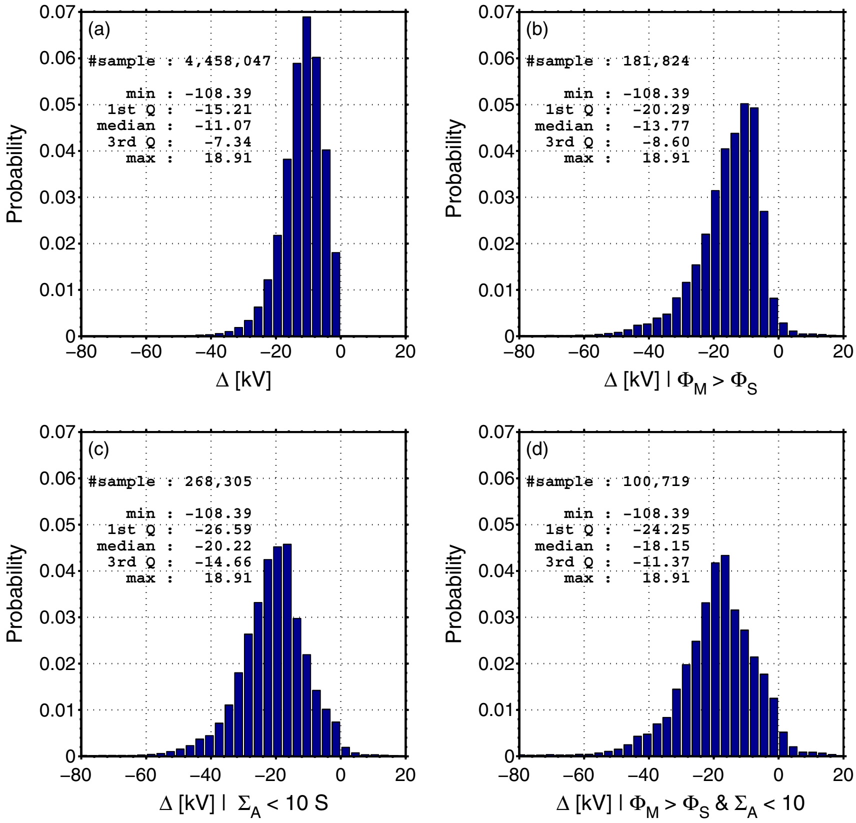

Figure 8. Histograms of Δ (a), a subset of Δ satisfying $\Phi_M > \Phi_S$ (b), a subset of Δ satisfying $\Sigma_A < 10$ S (c), and a subset of Δ satisfying $\Phi_M > \Phi_S$ and $\Sigma_A < 10$ S (d) for 1 min solar wind observation from 1999 to 2009. The text in a panel shows the summary statistics of the plotted quantity.

even though the two models gave fundamentally different predictions for the case of 15 May 2005, the difference of the predicted values was still not large enough in magnitude to argue that one model is better than the other by directly comparing $\Phi_{S\text{-}H}$ and $\Phi_{K\text{-}R}$ with data.

[16] There are two factors that complicate comparisons between the Siscoe-Hill model and the Kivelson-Ridley model. One is the concurrent action of the mechanisms of the Siscoe-Hill model and the Kivelson-Ridley model in cases producing saturation. The other is the feedback of magnetotail activity. We comment on these two matters.

[17] The mechanisms identified as the reasons for saturation in the two models, i.e., feedback of the Region 1 current that reduces the reconnection rate and reflection of the incident electric field that reduces the transmitted electric field are both likely to act during a saturation interval. *Siscoe* [2011] argued that the two models probably should be regarded not as different theories but as alternative formulations of the same basic idea. He further argued that the Siscoe-Hill model formulates the basic idea, while the Kivelson-Ridley model gives a specific instance of it. The consistency between the two models during a saturation interval suggests that the process described by *Siscoe et al.* [2002] is likely to occur concurrently with that described by *Kivelson and Ridley* [2008]. However, we do not support the view of *Siscoe* [2011] that the Kivelson-Ridley model should be viewed as a specific instance of the Siscoe-Hill model. On the one hand, an instance on 15 May 2005 is found, for which after 06:00 UT the Siscoe-Hill model predicts no saturation but the Kivelson-Ridley model predicts saturation. On the other hand, it is difficult to believe that the magnetic field cancellation at low-latitude magnetopause resulting from enhanced Region 1 currents is the same as the partial wave reflection on a newly reconnected field line due to the dominance of solar wind impedance over the ionospheric

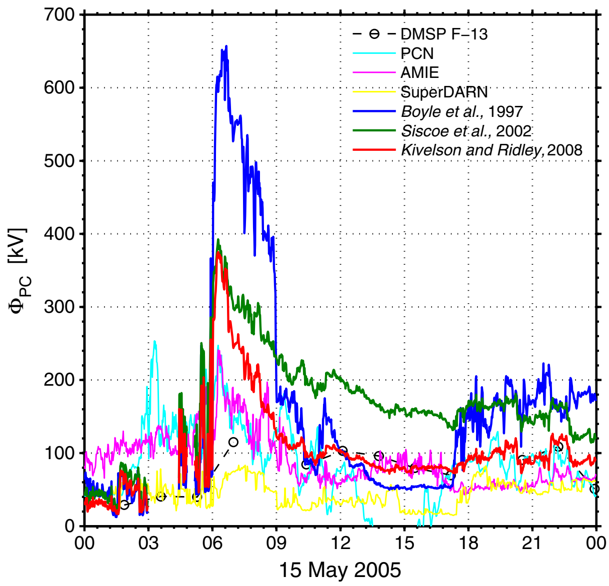

Figure 9. As in Figure 1 for a different case on 15 May 2005.

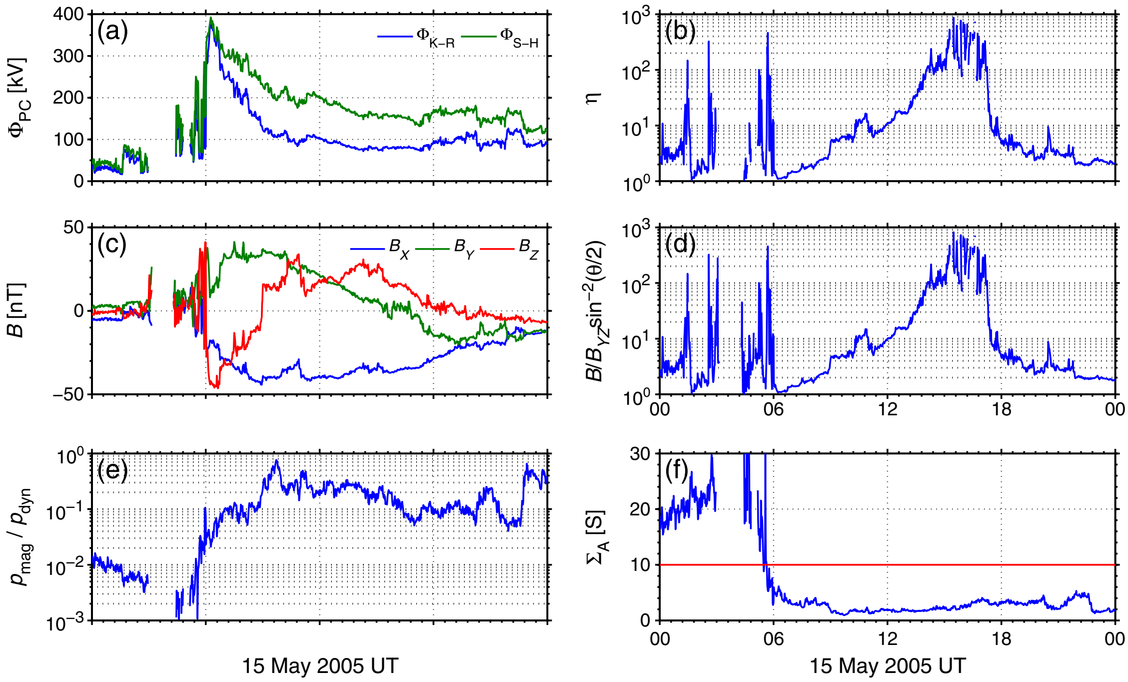

Figure 10. The predicted cross polar cap potentials and the relevant parameters on 15 May 2005. Plotted are the time series of $\Phi_{K\text{-}R}$ and $\Phi_{S\text{-}H}$ (a), η (equation (32)) (b), IMF in GSM coordinates (c), $B/B_{YZ}\sin^{-2}\theta/2$ (d), the ratio of p_{mag} to p_{dyn} (e), and the solar wind Alfvén conductance Σ_A (f).

impedance. We think it likely that one process plays a key role but that it is unlikely that we will be able to establish unambiguously from observation which is dominant.

[18] It is worth noting that neither model predicts the full cross polar cap potential (e.g., Figure 1). The cross polar cap potential arises from the sum of all convective flows in the polar ionosphere. In addition to the convection initiated by the solar wind and IMF, there are other sources of the convective flows. For example, *Gao et al.* [2012c] found that the polar cap dynamics also respond to magnetotail energy unloading, whose contribution is about half of that of solar wind driving. Thus, magnetotail activity is expected to contribute significantly to the cross polar cap potential. However, both the Siscoe-Hill model and the Kivelson-Ridley model are models driven by the solar wind. They make no attempt to include the phenomenology of the magnetotail and do not ascribe any particular importance to reconnection in the tail. A direct consequence is that the measured Φ_{PC} is more dynamic (and often larger) than Φ_{PC} predicted by either model. For example, as shown in Figure 1, the measured Φ_{PC}s by AMIE (magenta line) and PC index (cyan line) varied more drastically than the predicted Φ_{PC}s from Siscoe-Hill model (green line) and Kivelson-Ridley model (red line) in the saturation interval (11:00 UT to 20:00 UT). The more dynamic nature of the measurements than the model predictions is confirmed by other cases (e.g., Figures 5 and 9). This further complicates the comparison of the two models.

4. Discussion and Conclusions

[19] It has been noted in previous studies [e.g., *Lavraud and Borovsky*, 2008; *Siscoe*, 2011] that the cross polar cap potential predicted by *Siscoe et al.* [2002] is similar to that predicted by *Kivelson and Ridley* [2008]. In this paper, we examine the similarities and differences between the two models mathematically and compare the predictions to measurements. We find that the mathematical formula of the Kivelson-Ridley model is similar to that of the Siscoe-Hill model. The difference can be summarized in an η factor (equation (25) vs. equation (34)). Using the saturation cases of *Gao et al.* [2012c], we compare the model predictions with the measurements of AMIE, DMSP, PC index, and SuperDARN. We find that, as expected, the model predictions are very close to each other, although the measurements from different techniques are quite different. A systematic survey of the differences in model predictions from 1999 to 2009 shows that, on average, $\Phi_{K\text{-}R}$ is smaller than $\Phi_{S\text{-}H}$ by roughly 10 kV. Given the uncertainties of the measurements, such a difference is not large enough to support one model over the other. In one exceptional event, the difference between $\Phi_{S\text{-}H}$ and $\Phi_{K\text{-}R}$ was as large as 100 kV. However, even for this case, it was still not possible to establish that one model is to be preferred over the other by comparing with observations.

[20] *Siscoe et al.* [2002] propose that it is the feedback of the Region 1 current that reduces the reconnection rate, which eventually limits the rate of flux transfer from the solar wind to the magnetotail, resulting in the saturation of Φ_{PC}. However, *Kivelson and Ridley* [2008] argue that the saturation of Φ_{PC} is caused by the reflection of the Alfvén waves incident from the solar wind, when the impedance of the solar wind across the polar cap field lines dominates the impedance of the ionosphere. These two processes co-occur in a saturation interval and lead to very similar predictions of Φ_{PC}. Thus, it is impossible to tell which is responsible for the saturation of Φ_{PC} from observations.

[21] Contributions from magnetotail activity further complicate the comparison of the models. According to *Gao et al.* [2012c], polar cap dynamics are significantly

influenced by the magnetotail energy unloading, and so is Φ_{PC}. [see also *Gao*, 2012b; *Gao et al*., 2012a, 2012b]. Since both the Siscoe-Hill model and the Kivelson-Ridley model are driven models that do not incorporate the effects of magnetotail activity, it is unlikely that either prediction will be fully consistent with measurements. The measured Φ_{PC} is typically more dynamic than that predicted from the models, an observation that is confirmed from Figures 1, 4, and 7. Thus, not only is it difficult to find events in which the solar wind input implies significantly different predictions from the contending theories but also the theories predict only a portion of the polar cap response, making it even more challenging to find events in which data could support one theory over the other.

[22] **Acknowledgments.** YG acknowledges support from NASA under grant UCB/NASA NAS 5-02099. He thanks Dr. R. L. McPherron, Dr. K. K. Khurana, and Dr. T-S. Hsu for helpful discussions. We are indebted to Dr. A. J. Ridley for his technical support in running the AMIE software. We are grateful to Dr. J. M. Weygand for propagating the ACE data from $L1$ to $X_{GSM} = 17R_E$. The propagated data were downloaded from the Virtual Magnetospheric Observatory (VMO) at http://vmo.igpp.ucla.edu/. We are also grateful to Dr. M. R. Hairston for the help in analyzing the DMSP Special Sensor-Ions, Electrons, and Scintillation (SSIES) data, which can be downloaded from http://cindispace.utdallas.edu/DMSP/. The northern PC index (PCN index) used in this study comes from magnetic data of Qaanaaq station (86.5° magnetic latitude) and is available at ftp://ftp.space.dtu.dk/WDC/indices/pnc. The SuperDARN data are provided by N. A. Frissell at Virginia Tech.

References

Baker, J. B. H., R. A. Greenwald, J. M. Ruohoniemi, K. Oksavik, J. W. Gjerloev, L. J. Paxton, and M. R. Hairston (2007), Observations of ionospheric convection from the Wallops SuperDARN radar at middle latitudes, *J. Geophys. Res.*, *112*(A1), A01303, doi:10.1029/2006JA011982.

Borovsky, J. E., B. Lavraud, and M. M. Kuznetsova (2009), Polar cap potential saturation, dayside reconnection, and changes to the magnetosphere, *J. Geophys. Res.*, *114*(A3), A03224.

Boyle, C. B., P. H. Reiff, and M. R. Hairston (1997), Empirical polar cap potentials, *J. Geophys. Res.*, *102*(A1), 111–125, doi:10.1029/96ja01742.

Cleveland, W. S. (1979), Robust locally weighted regression and smoothing scatterplots, *JASA*, *74*(368), 829–836, doi:10.2307/2286407.

Ebihara, Y., N. Nishitani, T. Kikuchi, T. Ogawa, K. Hosokawa, M. C. Fok, and M. F. Thomsen (2009), Dynamical property of storm time subauroral rapid flows as a manifestation of complex structures of the plasma pressure in the inner magnetosphere, *J. Geophys. Res.*, *114*(A1), A01306, doi:10.1029/2008JA013614.

Gao, Y. (2012a), Comparing the cross polar cap potentials measured by SuperDARN and AMIE during saturation intervals, *J. Geophys. Res.*, *117*(A8), A08325, doi:10.1029/2012JA017690.

Gao, Y. (2012b), On anomalous departures from a linear relation between the polar cap index and its controlling factors in solar wind and magnetotail, *J. Geophys. Res.*, *117*(A6), A06201, doi:10.1029/2012JA017721.

Gao, Y., M. G. Kivelson, and R. J. Walker (2012a), The linear dependence of polar cap index on its controlling factors in solar wind and magnetotail, *J. Geophys. Res.*, *117*(A5), A05213, doi:10.1029/2011JA017229.

Gao, Y., M. G. Kivelson, R. J. Walker, and J. M. Weygand (2012b), Long-term variation of driven and unloading effects on polar cap dynamics, *J. Geophys. Res.*, *117*(A2), A02203, doi:10.1029/2011JA017149.

Gao, Y., M. G. Kivelson, A. J. Ridley, J. M. Weygand, and R. J. Walker (2012c), Utilizing the polar cap index to explore strong driving of polar cap dynamics, *J. Geophys. Res.*, *117*(A7), A07213, doi:10.1029/2011JA017087.

Hairston, M. R., R. A. Heelis, and F. J. Rich (1998), Analysis of the ionospheric cross polar cap potential drop using DMSP data during the National Space Weather Program study period, *J. Geophys. Res.*, *103*(A11), 26337–26347, doi:10.1029/97JA03241.

Hairston, M. R., T. W. Hill, and R. A. Heelis (2003), Observed saturation of the ionospheric polar cap potential during the 31 March 2001 storm, *Geophys. Res. Lett.*, *30*(6), 1325, doi:10.1029/2002GL015894.

Hill, T. W., A. J. Dessler, and R. A. Wolf (1976), Mercury and Mars: The role of ionospheric conductivity in the acceleration of magnetospheric particles, *Geophys. Res. Lett.*, *3*(8), 429–432, doi:10.1029/GL003i008p00429.

Jiang, F., M. G. Kivelson, R. J. Walker, K. K. Khurana, V. Angelopoulos, and T. Hsu (2011), A statistical study of the inner edge of the electron plasma sheet and the net convection potential as a function of geomagnetic activity, *J. Geophys. Res.*, *116*(A6), A06215, doi:10.1029/2010JA016179.

Kan, J. R., and L. C. Lee (1979), Energy coupling function and solar wind-magnetosphere dynamo, *Geophys. Res. Lett.*, *6*, 577–580.

Kivelson, M. G., and A. J. Ridley (2008), Saturation of the polar cap potential: Inference from Alfvén wing arguments, *J. Geophys. Res.*, *113*(A5), A05214, doi:10.1029/2007JA012302.

Lavraud, B., and J. E. Borovsky (2008), Altered solar wind-magnetosphere interaction at low Mach numbers: Coronal mass ejections, *J. Geophys. Res.*, *113*(A9), A00B08, doi:10.1029/2008JA013192.

Merkin, V. G., A. S. Sharma, K. Papadopoulos, G. Milikh, J. Lyon, and C. Goodrich (2005), Global MHD simulations of the strongly driven magnetosphere: Modeling of the transpolar potential saturation, *J. Geophys. Res.*, *110*(A9), A09203, doi:10.1029/2004JA010993.

Merkine, V. G., K. Papadopoulos, G. Milikh, A. S. Sharma, X. Shao, J. Lyon, and C. Goodrich (2003), Effects of the solar wind electric field and ionospheric conductance on the cross polar cap potential: Results of global MHD modeling, *Geophys. Res. Lett.*, *30*(23), 2180, doi:10.1029/2003GL017903.

Nagatsuma, T. (2002), Saturation of polar cap potential by intense solar wind electric fields, *Geophys. Res. Lett.*, *29*(10), 1422, doi:10.1029/2001GL014202.

Ober, D. M., N. C. Maynard, and W. J. Burke (2003), Testing the Hill model of transpolar potential saturation, *J. Geophys. Res.*, *108*(A12), 1467, doi:10.1029/2003JA010154.

Raeder, J., Y. L. Wang, T. J. Fuller-Rowell, and H. J. Singer (2001), Global simulation of magnetospheric space weather effects of the Bastille day storm, *Sol. Phys.*, *204*(1–2), 323–337, doi:10.1023/A:1014228230714.

Richmond, A. D., and Y. Kamide (1988), Mapping electrodynamic features of the high-latitude ionosphere from localized observations: Technique, *J. Geophys. Res.*, *93*(A6), 5741–5759, doi:10.1029/JA093iA06p05741.

Richmond, A. D., et al. (1988), Mapping electrodynamic features of the high-latitude ionosphere from localized observations: Combined incoherent-scatter radar and magnetometer measurements for January 18–19, 1984, *J. Geophys. Res.*, *93*(A6), 5760–5776, doi:10.1029/JA093iA06p05760.

Ridley, A. J. (2005), A new formulation for the ionospheric cross polar cap potential including saturation effects, *Ann. Geophys.*, *23*(11), 3533–3547, doi:10.5194/angeo-23-3533-2005.

Ridley, A. J., and E. A. Kihn (2004), Polar cap index comparisons with AMIE cross polar cap potential, electric field, and polar cap area, *Geophys. Res. Lett.*, *31*, L07801.

Ruohoniemi, J. M., and K. B. Baker (1998), Large-scale imaging of high-latitude convection with Super Dual Auroral Radar Network HF radar observations, *J. Geophys. Res.*, *103*(A9), 20,797–20,811, doi:10.1029/98ja01288.

Russell, C. T., G. Lu, and J. G. Luhmann (2000), Lessons from the ring current injection during the September 24, 25, 1998 storm, *Geophys. Res. Lett.*, *27*(9), 1371–1374, doi:10.1029/1999GL003718.

Shepherd, S. G., R. A. Greenwald, and J. M. Ruohoniemi (2002), Cross polar cap potentials measured with Super Dual Auroral Radar Network during quasi-steady solar wind and interplanetary magnetic field conditions, *J. Geophys. Res.*, *107*(A7), 1094, doi:10.1029/2001JA000152.

Siscoe, G. L. (2011), Aspects of global coherence of magnetospheric behavior, *J. Atmos. Sol-Terr. Phy.*, *73*(4), 402–419, doi:10.1016/j.jastp.2010.11.005.

Siscoe, G. L., J. Raeder, and A. J. Ridley (2004), Transpolar potential saturation models compared, *J. Geophys. Res.*, *109*(A9), A09203, doi:10.1029/2003JA010318.

Siscoe, G. L., G. M. Erickson, B. U. Ö. Sonnerup, N. C. Maynard, J. A. Schoendorf, K. D. Siebert, D. R. Weimer, W. W. White, and G. R. Wilson (2002), Hill model of transpolar potential saturation: Comparisons with MHD simulations, *J. Geophys. Res.*, *107*(A6), 1075, doi:10.1029/2001JA000109.

Troshichev, O. A., V. G. Andrezen, S. Vennerstrom, and E. Friis-Christensen (1988), Magnetic activity in the polar cap—A new index, *Planet. Space Sci.*, *36*, 1095–1102.

Troshichev, O. A., H. Hayakawa, A. Matsuoka, T. Mukai, and K. Tsuruda (1996), Cross polar cap diameter and voltage as a function of PC index and interplanetary quantities, *J. Geophys. Res.*, *101*, 13,429–13,436.

Weimer, D. R. (2004), Correction to "Predicting interplanetary magnetic field (IMF) propagation delay times using the minimum variance technique," *J. Geophys. Res.*, *109*(A12), A12104, doi:10.1029/2004JA010691.

Weimer, D. R., D. M. Ober, N. C. Maynard, M. R. Collier, D. J. McComas, N. F. Ness, C. W. Smith, and J. Watermann (2003), Predicting interplanetary magnetic field (IMF) propagation delay times using the minimum variance technique, *J. Geophys. Res.*, *108*(A1), 1026, doi:10.1029/2002JA009405.